

# The Phasor Transformer: Resolving Attention Bottlenecks on the Unit Circle

Dibakar Sigdel<sup>1\*</sup>

<sup>1</sup> Mindverse Computing LLC, WA 98087

March 19, 2026

## Abstract

Transformer models have redefined sequence learning, yet dot-product self-attention introduces a quadratic token-mixing bottleneck for long-context time-series. We introduce the **Phasor Transformer** block, a phase-native alternative representing sequence states on the unit-circle manifold  $S^1$ . Each block combines lightweight trainable phase-shifts with parameter-free Discrete Fourier Transform (DFT) token coupling, achieving global  $\mathcal{O}(N \log N)$  mixing without explicit attention maps. Stacking these blocks defines the **Large Phasor Model (LPM)**. We validate LPM on autoregressive time-series prediction over synthetic multi-frequency benchmarks. Operating with a highly compact parameter budget, LPM learns stable global dynamics and achieves competitive forecasting behavior compared to conventional self-attention baselines. Our results establish an explicit efficiency-performance frontier, demonstrating that large-model scaling for time-series can emerge from geometry-constrained phase computation with deterministic global coupling, offering a practical path toward scalable temporal modeling in oscillatory domains.

## 1 Introduction

The Transformer architecture [17] fundamentally changed sequence modeling by replacing recurrent locality with global token interaction. This design unlocked large-scale pretraining and directly enabled the modern progression from bidirectional language encoders such as BERT [6] to autoregressive foundation models such as GPT-3 [2] and scaling-law-driven large language model (LLM) regimes [10, 9]. The same core design has also propagated into vision and multimodal systems, for example Vision Transformers [7], reinforcing the Transformer as a general-purpose sequence processor.

Despite this success, the dominant self-attention mechanism remains computationally expensive for long contexts because full query-key interactions scale quadratically with sequence length. This has motivated a broad line of efficient Transformer research [16], including sparse or structured attention (Sparse Transformer, Longformer, BigBird) [3, 1, 21], low-rank projections (Linformer) [18], kernelized approximations (Performer) [4], and systems-level optimizations such as FlashAttention [5]. These approaches reduce memory and latency costs, but in many settings they still trade exact global interaction, introduce approximation error, or require specialized kernels and hardware-aware tuning.

In parallel, another line of work demonstrates that explicit pairwise attention maps are not always necessary for effective token mixing. Fourier-based token-mixing methods such as FNet [11] show that global spectral transforms can recover much of Transformer performance

---

\*devdeep137@gmail.com

at substantially lower complexity, replacing learned dense interaction with deterministic global mixing in  $O(N \log N)$ . This observation is particularly relevant for time-series modeling, where periodicity, phase relations, and frequency structure are first-class signals rather than incidental features.

Time-series forecasting and sequence generation have therefore seen a rapid expansion of Transformer-inspired architectures, including Temporal Fusion Transformers [12], Informer [22], Autoformer [20], FEDformer [23], PatchTST [13], and TimesNet [19]. These models improve horizon length and predictive quality through decomposition, sparse attention, patching, or spectral modules. However, most still operate primarily in Euclidean latent spaces, where phase behavior is encoded indirectly through learned projections rather than represented natively.

This motivates a complementary perspective based on complex-valued and phase-native computation. Complex-domain neural modeling has long suggested that magnitude-phase factorization can offer representational and optimization advantages in oscillatory settings [8, 14]. From a geometric viewpoint, representing tokens directly on the unit circle  $S^1$  (and, for sequences, on the torus  $\mathbb{T}^N$ ) provides bounded state evolution with explicit phase semantics. In such a representation, global Fourier mixing corresponds to physically interpretable interference rather than an implicit consequence of dense Euclidean matrix multiplication.

In this manuscript, we first introduce a **Phasor Transformer** block as a phase-native alternative to dense attention layers. Each block combines trainable phase-shift layers with deterministic global DFT token mixing, preserving long-range coupling with subquadratic complexity and significantly fewer trainable parameters than dense attention counterparts, building directly upon the foundational computational primitives formalized in the PhasorFlow framework [15]. We then define the **Large Phasor Model (LPM)** as a deep stack of these Phasor Transformer blocks. Conceptually, this sequence unifies three desirable properties: (i) global context propagation without explicit  $N \times N$  attention maps, (ii) compact and interpretable phase-parameterized blocks, and (iii) natural alignment with periodic and quasi-periodic temporal dynamics.

The importance of this direction is not only computational. For many real-world sequences, including biosignals, finance, climate, and industrial telemetry, predictive structure is often carried by phase synchronization, oscillatory coupling, and cross-scale frequency interactions. A large phasor model can therefore be a game changer for time-series modeling by moving these quantities from emergent latent artifacts to primary state variables. This shift enables a new scaling trajectory: increasing depth and context in a geometrically constrained manifold where global mixing is deterministic, parameter growth is controlled, and interpretability remains tied to explicit circuit operations.

Our contributions are threefold. First, we formalize token mixing and sequence transformation on the continuous unit-circle manifold for large-scale sequence modeling. Second, we define the LPM architecture as a deep stack of phasor blocks with deterministic DFT-mediated global propagation and lightweight trainable phase gates. Third, we empirically benchmark LPM against conventional Transformer baselines on time-series tasks to quantify efficiency, scalability, and accuracy trade-offs. Together, these results position LPM as a practical and theoretically grounded candidate for the next generation of long-context temporal foundation models.

## 2 Theory

This section first develops the Phasor Transformer block as a phase-native sequence operator on the torus manifold, then defines LPM as its deep stacked form. The presentation is organized into four components: (i) state geometry, (ii) unitary operators, (iii) single-block token mixing, and (iv) deep composition with inter-block pull-back.

## 2.1 Dense Euclidean Baseline and Motivation

Standard self-attention computes pairwise token interactions through

$$\text{Attention}(Q, K, V) = \text{Softmax}\left(\frac{QK^\top}{\sqrt{d_k}}\right)V, \quad (1)$$

which induces an explicit  $T \times T$  interaction map for context length  $T$ . This yields quadratic coupling overhead in sequence length and motivates a deterministic global mixer that avoids learned dense pairwise maps.

## 2.2 Phasor Token States on $\mathbb{T}^N$

LPM represents token coordinates as phases on  $S^1$ . For a context of length  $N$  (equivalently  $T$  in implementation notation), the encoded state is

$$\mathbf{z} = \left(e^{i\phi_1}, \dots, e^{i\phi_N}\right)^\top \in \mathbb{T}^N \subset \mathbb{C}^N, \quad (2)$$

where  $\phi_t \in [-\pi, \pi]$  denotes token phase at coordinate  $t$ .

**Definition 2.1** (Phasor Token State Manifold). *For context length  $N$ , the admissible state manifold is*

$$\mathcal{M}_{\text{LPM}} = \mathbb{T}^N = \{\mathbf{z} \in \mathbb{C}^N : |z_t| = 1, t = 1, \dots, N\}. \quad (3)$$

We reserve  $\phi$  for state coordinates and use  $\theta$  for trainable operator parameters.

**Definition 2.2** (Ambient Interference Space). *Although encoded inputs lie on  $\mathbb{T}^N$ , linear mixing acts on the ambient vector space  $\mathbb{C}^N$ . Thus unitary maps preserve global  $\ell^2$  energy but need not preserve coordinatewise unit modulus.*

## 2.3 Unitary Gate Primitives

The LPM block uses two operator classes:

$$S(\boldsymbol{\theta}) = \text{diag}\left(e^{i\theta_1}, \dots, e^{i\theta_T}\right), \quad F_T[k, n] = \frac{1}{\sqrt{T}}e^{-i2\pi kn/T}. \quad (4)$$

Here,  $S(\boldsymbol{\theta}) \in U(1)^T \subset U(T)$  is a coordinatewise phase rotation, and  $F_T \in U(T)$  is a global DFT mixer.

Applying  $F_T$  to a phasor state yields

$$f_k = \frac{1}{\sqrt{T}} \sum_{n=0}^{T-1} e^{i\phi_n} e^{-i2\pi kn/T}, \quad (5)$$

so every output coordinate depends on every token phase.

**Proposition 2.1** (Spectral Mixing Preserves Energy, Not Coordinatewise Modulus). *Let  $\mathbf{z} \in \mathbb{T}^N$  and  $F_T \in U(T)$ . Then*

$$\|F_T \mathbf{z}\|_2 = \|\mathbf{z}\|_2 = \sqrt{T}, \quad (6)$$

while in general  $F_T \mathbf{z} \notin \mathbb{T}^N$  because coordinatewise constraints  $|(F_T \mathbf{z})_k| = 1$  need not hold.

## 2.4 Single-Block Phasor Transformer Operator

A single LPM block is

$$\mathcal{B}(\boldsymbol{\theta}) = S(\boldsymbol{\theta}^{\text{post}}) F_T S(\boldsymbol{\theta}^{\text{pre}}), \quad (7)$$

where pre/post phase shifts are trainable and  $F_T$  is parameter-free global token coupling.

**Definition 2.3** (Phasor Transformer Block). *For context length  $T$ , a block is*

$$\mathcal{B}(\boldsymbol{\theta}) = S(\boldsymbol{\theta}^{\text{post}}) F_T S(\boldsymbol{\theta}^{\text{pre}}), \quad (8)$$

with exactly  $2T$  trainable phase parameters.

The single-block operator layout is shown in Figure 1.

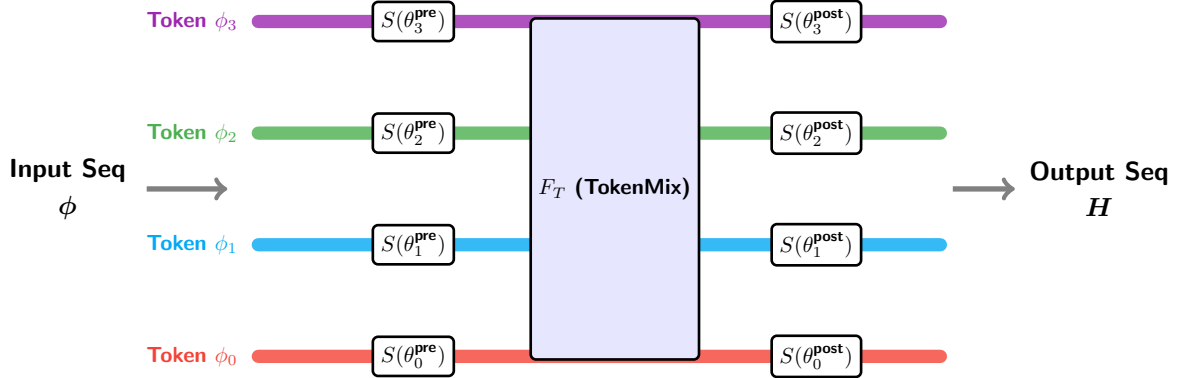


Figure 1: Single-block Phasor Transformer used in LPM. Global token interaction is induced by deterministic DFT interference ( $F_T$ ), while learnable pre/post shift layers provide lightweight phase adaptation.

**Theorem 2.1** (Linear-Parameter Global Mixing in LPM). *Let an LPM of depth  $D$  process context length  $T$  by stacking  $D$  blocks  $\mathcal{B}_1, \dots, \mathcal{B}_D$  with one readout phase projection. Then:*

1. the trainable parameter count scales as  $(2D + 1)T$ ;
2. each block performs global token interaction through  $F_T$  without constructing a dense  $T \times T$  attention map;
3. the dominant token-mixing complexity per block is  $\mathcal{O}(T \log T)$ .

Hence LPM achieves globally coupled sequence mixing under linear parameter growth in context length.

**Proposition 2.2** (Pull-Back Boundedness for Inter-Block States). *For raw phase coordinate  $\phi_{\text{raw}} \in \mathbb{R}$ , define the pull-back map*

$$\Phi_{\text{norm}}(\phi_{\text{raw}}) = \arcsin(\sin(\phi_{\text{raw}})). \quad (9)$$

Then  $\Phi_{\text{norm}}(\phi_{\text{raw}}) \in [-\pi/2, \pi/2]$  for all inputs, so every inter-block state is deterministically folded back into a bounded principal interval before the next spectral mixing stage.

**Corollary 2.2** (Parameter-Efficiency Regime of LPM). *Under the block structure above, replacing dense self-attention with DFT token mixing yields a model class whose trainable parameter count grows linearly with context length while retaining global token coupling. Therefore LPM admits a compact long-context regime where parameter budgets are substantially smaller than conventional quadratic-attention designs.*

## 2.5 From Single-Stack to Multi-Stack LPM

Purely unitary compositions preserve global energy in  $\mathbb{C}^T$  but can push intermediate thread magnitudes away from the unit-circle manifold. To maintain stable deep composition, LPM introduces a phase-domain pull-back nonlinearity between blocks,

$$\Phi_{\text{norm}} = \arcsin(\sin(\phi_{\text{raw}})), \quad (10)$$

which folds angular states back into a bounded principal interval before the next DFT-mixing stage. In this way, each block begins from a torus-compatible phase representation, evolves through complex interference under unitary mixing, and is then re-embedded into a bounded phase chart before the next block.

With this inter-block renormalization, a depth- $D$  LPM is written as a stacked composition

$$\text{LPM}(\boldsymbol{\theta}) = \mathcal{B}_D(\boldsymbol{\theta}_D) \circ \cdots \circ \mathcal{B}_1(\boldsymbol{\theta}_1) \circ U_{\text{enc}}(\mathbf{x}), \quad (11)$$

where each block applies pre-shift, global mixing, and post-shift operations. This gives a mathematically coherent route from single-block token mixing to deep long-context sequence operators on phase manifolds.

The operator-level multi-stack layout is shown in Figure 2.

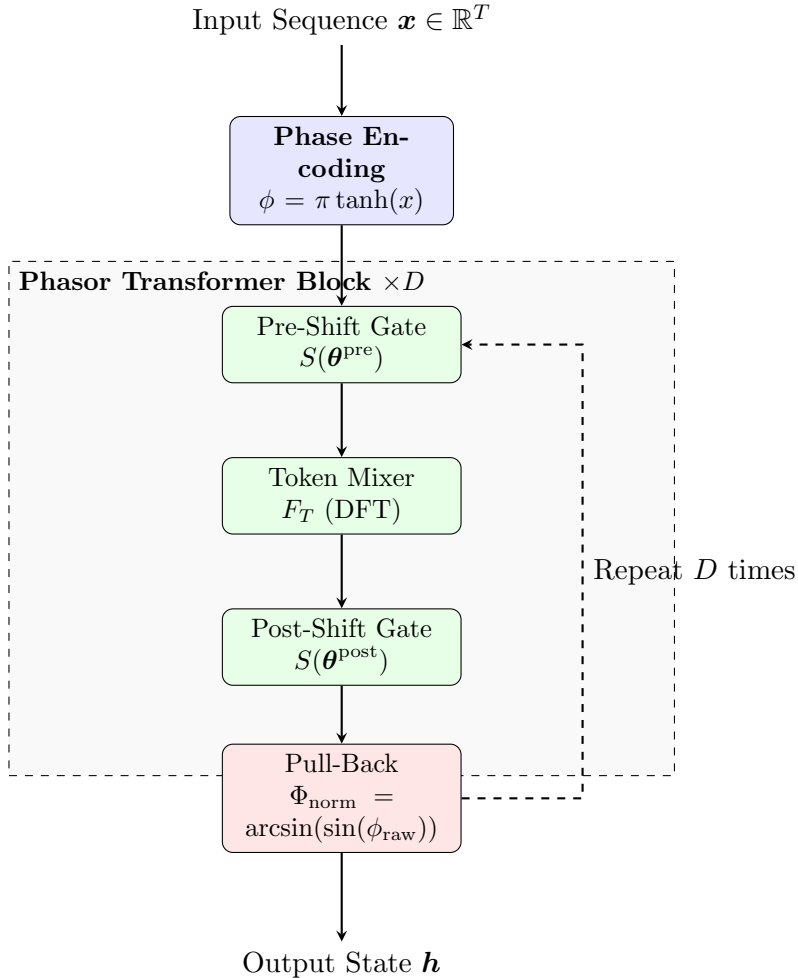


Figure 2: Multi-stack LPM transformer schematic. Each block applies pre-shift, DFT token mixing, and post-shift operations, followed by pull-back normalization before the next block.

### 3 Method

This section presents the practical LPM workflow in the same stage-based structure used throughout PhasorFlow: Stage 1 data encoding, Stage 2 variational token mixing, and Stage 3 deterministic readout.

#### 3.1 Dataset and Experimental Splits

To precisely evaluate the sequence modeling capabilities of the Large Phasor Model, we utilize a controlled synthetic dataset constructed from autoregressive, multi-frequency oscillatory sequences injected with additive Gaussian noise. This controlled environment isolates the model’s ability to learn and extrapolate complex superposition dynamics from background stochasticity. Each generated sample strictly provides a fixed-length historical context window mapped directly to a one-step-ahead target value. For our primary evaluations of the core LPM architecture, we institute a standard temporal context length of  $T = 10$ . In contrast, for rigorous architectural benchmarking against baseline models, we deliberately extend the context horizon (e.g.,  $T = 32$ ) while preserving the identical underlying generation process, effectively testing the model’s capacity to maintain phase coherence over extended temporal dependencies.

To ensure the integrity of the evaluation and prevent data leakage, all experimental trials are executed across statically fixed partitions for training, validation, and testing. Crucially, the test split is entirely sequestered from the optimization process, functioning strictly as a held-out oracle for final reporting and generalization assessment.

#### 3.2 Data Encoding

Rather than processing raw Euclidean features directly, the LPM enforces a strict geometric prior by mapping all inputs onto a bounded periodic manifold prior to learning. Given a temporal history window defined as  $\mathbf{x} = (x_1, \dots, x_T)$ , the raw sequence values undergo a symmetric amplitude-normalization mapping. The values are scaled relative to the maximum absolute amplitude observed within the window and subsequently projected into bounded phase coordinates:

$$\phi_t = \frac{x_t}{\max|\mathbf{x}|} \cdot \frac{\pi}{2}, \quad t = 1, \dots, T. \quad (12)$$

This projection limits the resultant phase angles to the principal interval  $[-\pi/2, \pi/2]$ . Subsequently, these continuous geometric angles are lifted onto the unit circle in the complex plane, constructing the encoded phasor input state:

$$\mathbf{z}_{\text{in}} = (e^{i\phi_1}, \dots, e^{i\phi_T})^\top \in \mathbb{T}^N, \quad N = T. \quad (13)$$

This deterministic encoding stage operates entirely externally to the trainable parameters of the phasor circuit. By initializing every forward pass strictly on the surface of the  $N$ -Torus ( $\mathbb{T}^N$ ), the architecture guarantees that deep oscillatory interference representations are structurally sheltered from the unconstrained magnitude explosions typical of deep networks operating in standard Euclidean space.

#### 3.3 Variational Phasor Transformer Layer

Following the initial data encoding, the temporal sequence is processed through stacked Variational Phasor Transformer blocks. Unlike standard attention-based transformers that rely on quadratic pairwise scalar dot-products, each LPM block computes a global token mixing operation using a parameter-free Discrete Fourier Transform (DFT), flanked by trainable pre- and post-shift layers. Mathematically, a single block  $\mathcal{B}(\boldsymbol{\theta})$  defines the transformation:

$$\mathcal{B}(\boldsymbol{\theta}) = S(\boldsymbol{\theta}^{\text{post}})F_T S(\boldsymbol{\theta}^{\text{pre}}). \quad (14)$$

The global unitary mixer  $F_T$  natively entangles the temporal features across the entire sequence context, while the parameterized Shift operators  $S(\boldsymbol{\theta})$  apply trainable, unentangled phase rotations that adapt the representation for the specific task. Over a deep architecture comprised of  $D$  layers, the signal propagates iteratively:

$$\mathbf{z}^{(\ell+1)} = \mathcal{B}(\boldsymbol{\theta}^{(\ell)}) \mathbf{z}^{(\ell)}, \quad \ell = 0, \dots, D - 1, \quad (15)$$

where the initial state is given by  $\mathbf{z}^{(0)} = \mathbf{z}_{\text{in}}$ . To ensure numerical stability when stacking numerous operations deep into the network, an intermediate pull-back normalization function:

$$\Phi_{\text{norm}}(\phi) = \arcsin(\sin \phi) \quad (16)$$

is inserted periodically between consecutive blocks. This geometry-preserving projection strictly bounds the phase angles back into the principal interval  $(-\pi, \pi]$  without discarding the underlying representational relational structures generated by the unitary mixers.

### 3.4 Deterministic Readout

The final architectural stage maps the deep phasor representation back into the Euclidean target domain. After the sequence is processed by the final transformer block, a designated terminal readout thread—typically corresponding to the final timestep  $T$  in the context window—is isolated for decoding. The target scalar value  $\hat{x}_{T+1}$  is predicted by extracting the angle of this output phasor and reversing the initial mapping scale:

$$\hat{x}_{T+1} = \phi_{\text{out},0} \cdot \frac{\max |\mathbf{x}|}{\pi/2}, \quad (17)$$

where  $\phi_{\text{out},0} = \arg(z_{\text{out},0})$  represents the exact phase of the primary output thread. This deterministic projection avoids the necessity of a dense, multi-layer perceptron readout head, drastically reducing final-stage parameter overhead while preserving the structural interpretability of the model.

### 3.5 Optimization Protocol

Model optimization is implemented in PyTorch, leveraging the framework’s continuous Auto-grad capabilities directly over the complex phase parameters  $\boldsymbol{\theta}$ . Rather than relying on discrete gradients or complex approximations, the network is trained end-to-end using standard gradient descent schema. Unless otherwise noted in specific ablations, we employ the Adam optimizer with a fixed learning rate schedule and epoch budget.

A standard training iteration follows the same stage order as the model design. The raw context window is first transformed through amplitude-normalized phase encoding. Forward propagation then applies stacked Variational Phasor Transformer blocks to produce global token mixing and localized phase shifts. Next, deterministic readout extracts the predicted scalar value from the terminal phase angle. The regression loss (typically Mean Squared Error) is computed against the autoregressive ground-truth target, and gradients are backpropagated through the pull-back operators into the shift parameters. For extended deep-stack runs, this protocol is kept fixed; only network depth and rollout horizon are varied.

### 3.6 Inference, Rollout, and Metrics

Inference is conducted sequentially. A one-step inference pass predicts the single value  $x_{T+1}$  directly from the supplied final tracking context window. For multi-step forecasting scenarios, we utilize an autoregressive rollout strategy wherein the model appends its own previous predictions to the tail of the sequence, systematically shifting the context window forward to achieve the desired forecast horizon (e.g., a 20-step rollout used during deep-stack evaluations).

To quantitatively benchmark the model’s performance, we report standard regression metrics including Mean Squared Error (MSE) and Mean Absolute Error (MAE), dictated by the specific experiment topology. Alongside these core accuracy metrics, we systematically document empirical convergence curves, total trainable parameter counts, and asymptotic token-mixing complexity relative to context length  $T$ . This comprehensive reporting explicitly characterizes the efficiency-accuracy trade-off achieved by the LPM’s reliance on  $\mathcal{O}(T \log T)$  unitary Fourier mixing over standard quadratic  $\mathcal{O}(T^2)$  self-attention protocols.

## 4 Results

### 4.1 Phasor Transformer Sequence Benchmarking

To evaluate phase-native token mixing on autoregressive forecasting, we tested the Phasor Transformer on synthetic multi-frequency sequences with additive Gaussian noise and context length  $T = 10$ .

Each sample contains randomized frequency components and noise, with the model predicting the next step  $T + 1$  from the observed context  $(x_1, \dots, x_T)$ . Inputs are linearly mapped into bounded phase coordinates in  $[-\pi/2, \pi/2]$ , preserving oscillatory structure while keeping the representation on a controlled angular domain.

Using `PhasorFlow`, we implemented a single FNet-style phasor block with trainable pre/post phase shifts around a parameter-free DFT mixer. Under this setting, the model uses 50 trainable scalar parameters. Readout is obtained from the output phase of the designated terminal thread.

#### 4.1.1 Continuous PyTorch Optimization

Optimization used `torch.optim.Adam` with 50 trainable phase parameters initialized uniformly in  $[-\pi/10, \pi/10]$ , learning rate  $\lambda = 0.05$ , and 100 training epochs.

Training MSE decreased from 1.6912 at initialization to 0.1624 by epoch 10 and reached 0.0563 at convergence, indicating stable optimization in the bounded phase representation.

#### 4.1.2 Test Set Evaluation and Parameter Efficiency

On the held-out test set, the model achieved a prediction MSE of 0.0705, showing that the compact phasor architecture can capture the dominant dynamics of this synthetic forecasting task.

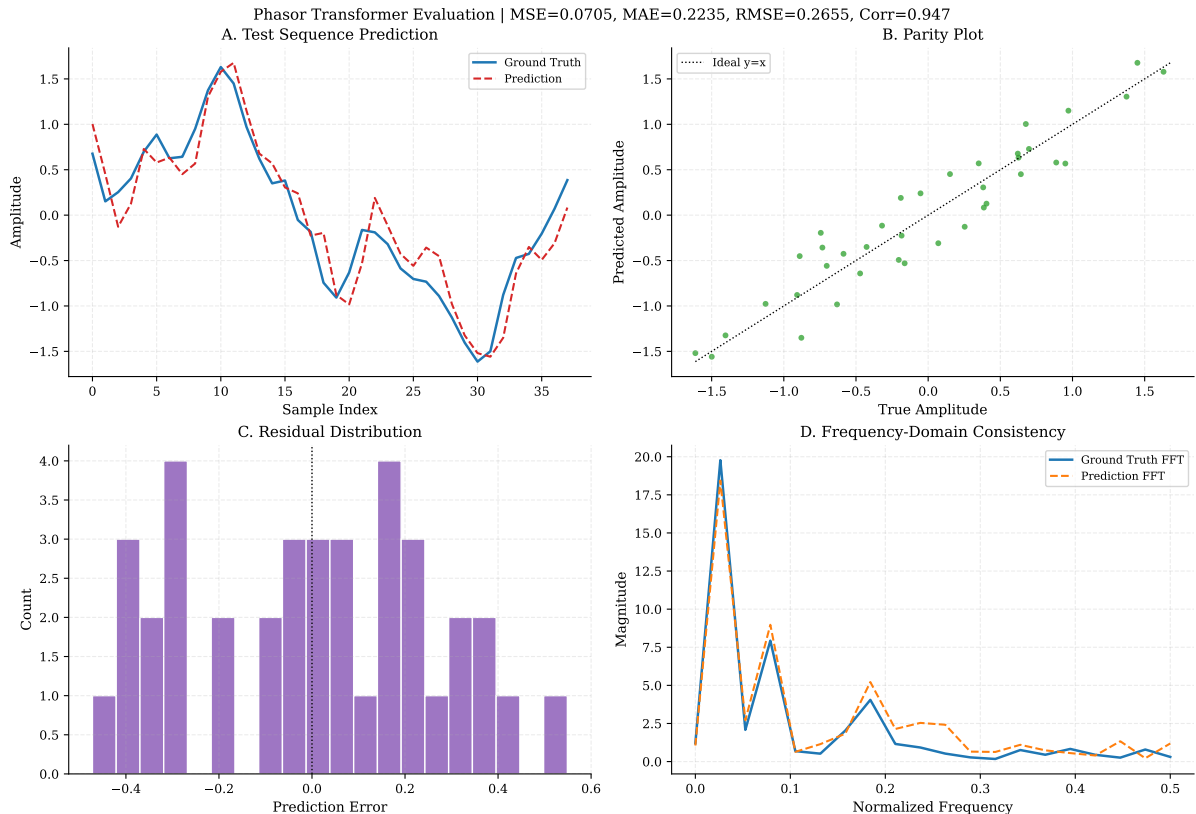


Figure 3: Phasor Transformer performance on sequence benchmarking, detailing the learning convergence and interpolation prediction capabilities.

Table 1: Sequence regression benchmark: Phasor Transformer vs Traditional Self-Attention.

Model	Test MSE	Trainable Params	Mixing Complexity
Phasor Transformer (DFT)	$\sim 0.07$	50	$\mathcal{O}(T \log T)$
PyTorch Transformer (Self-Attn)	$\sim 0.003$	$> 1,000$	$\mathcal{O}(T^2)$

As shown in Figure 3 and Table 1, the self-attention baseline attains lower test error on this task, while the phasor model operates with substantially fewer trainable parameters and subquadratic token-mixing complexity. These results highlight an explicit trade-off between predictive accuracy and model compactness in the evaluated setting.

Under the reported benchmark setting, the observed pair

$$(\text{Test MSE, Params}) \approx (0.07, 50) \quad (18)$$

supports an empirical efficiency-complexity tradeoff: useful autoregressive sequence modeling is attainable with logarithmic global mixing complexity and a parameter budget substantially below standard attention baselines.

## 5 Benchmarking Against Self-Attention

We compare a phasor token-mixing block based on parameter-free  $F_T$  against a standard PyTorch `nn.TransformerEncoderLayer` baseline.

The benchmark uses synthetic autoregressive multi-frequency sequences with context length  $N = 32$ . The PyTorch baseline embeds the 1D input into a 16-dimensional latent space with

4-head self-attention and a feed-forward sublayer. Both models are trained on 1,000 samples and evaluated on a disjoint 250-sample test split under the same regression objective.

**Benchmarking: Phasor Transformer vs. Traditional Self-Attention ( $N = 32$ )**

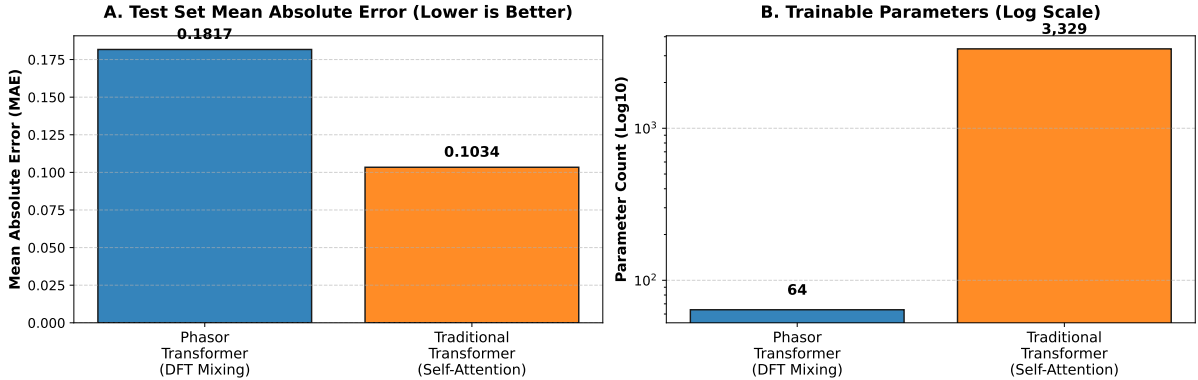


Figure 4: Empirical evaluation comparing the predictive capability (MAE) and training capacity of an  $S^1$  Phasor network relative to a deep Euclidean parameter space.

Model	Mixer	MAE	Trainable Params
<b>PhasorFlow Transformer</b>	DFT (global)	0.1817	<b>64 angles</b>
PyTorch (Self-Attention)	4-head attention	0.1034	<b>3,329 floats</b>

Table 2: Sequence Global Correlation Prediction Benchmarks ( $N = 32$  context length)

The self-attention baseline reaches lower MAE (0.1034), while the phasor model achieves MAE 0.1817 with 64 trainable angles. This result indicates reduced parameter count at the cost of some predictive accuracy in the tested configuration (Figure 4).

The practical implication is a complexity-profile trade-off: self-attention provides stronger accuracy on this benchmark but carries quadratic token-mixing costs, whereas the phasor design uses deterministic FFT-based global mixing with  $\mathcal{O}(N \log N)$  complexity and a compact trainable footprint.

From Table 2, the ratio between PyTorch and Phasor trainable parameters is

$$\rho = \frac{3329}{64} \approx 52.0, \quad (19)$$

indicating that the benchmarked Phasor Transformer attains competitive sequence regression with approximately two orders less trainable capacity than the dense self-attention baseline.

## 6 Deep Stack Versus Deep Circuit: Geometric Pull-Back

Unitary token mixing preserves global energy in  $\mathbb{C}^T$  but does not by itself enforce torus-valued coordinates between blocks. In a deep circuit without intermediate correction, repeated linear mixing can push coordinate magnitudes away from unit-modulus geometry.

To stabilize deep compositions, LPM inserts an explicit inter-block pull-back nonlinearity in phase space.

### 6.1 Inter-Block Phase Renormalization

Rather than using generic Euclidean activations, the model applies a manifold-aware phase fold:

$$\Phi_{\text{norm}}(\phi_{\text{raw}}) = \arcsin(\sin(\phi_{\text{raw}})). \quad (20)$$

This maps raw phase coordinates to a bounded principal interval and creates a non-linear boundary between successive unitary blocks. The result is a deep stack where each block starts from a geometrically reconditioned phase representation before another global DFT mixing step.

## 6.2 Deep $D = 3$ FNet Generative Representation Training

To empirically isolate the autoregressive generative capacity of a stacked representation, we extracted an  $N = 16$  sequence context sampling over an explicitly harder target threshold (evaluating  $T + 1$  through  $T + 20$  dynamic independent generation horizons).

We mapped a  $D = 3$  deep phasor block stack, inserting  $\Phi_{\text{norm}} = \arcsin(\sin(\phi_{\text{raw}}))$  between consecutive DFT-mixing blocks. Across this configuration (112 trainable phase parameters), optimization remained stable throughout training.

The operator-level deep-stack layout is given earlier in Figure 2.

**Deep Sequence Representation Learning & Generative Capacity in Phase Topologies**

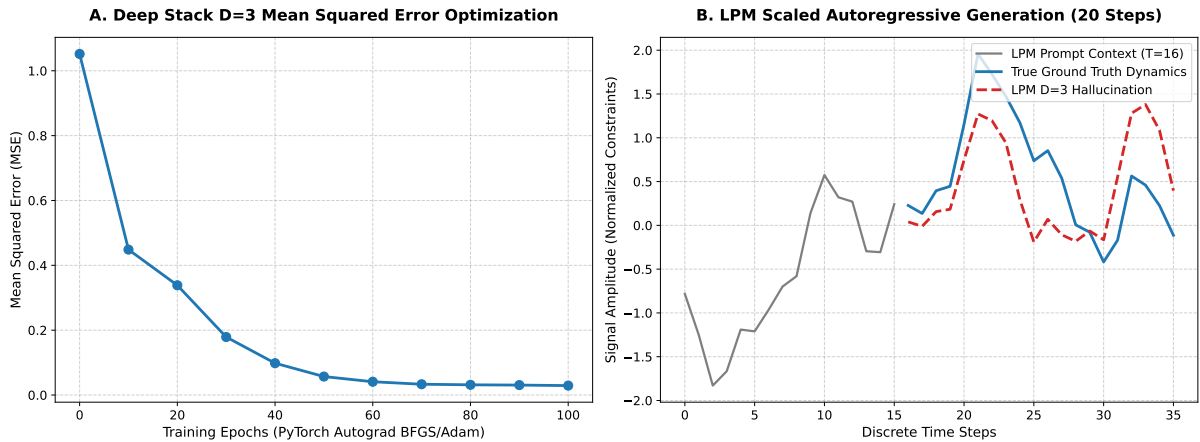


Figure 5: Generative Autoregressive rollout displaying independent extended interpolation capability following deep  $D = 3$  optimization.

As exhibited in Figure 5, standard PyTorch optimization reduced Mean Squared Error from 1.0519 to 0.029 (Figure 5A). On unseen prompts, the model produced a stable 20-step autoregressive continuation that tracked underlying target dynamics (Figure 5B).

Unlike a flat uninterrupted circuit, deep stacks impose explicit geometric boundaries between blocks. For the reported  $D = 3$  configuration, inserting  $\Phi_{\text{norm}} = \arcsin(\sin(\phi_{\text{raw}}))$  between blocks preserves bounded phase coordinates while retaining expressive non-linearity. The observed loss contraction and rollout fidelity support the deep-stack stabilization hypothesis.

## 7 Discussion

The results position LPM as a compact alternative for long-context sequence modeling where global coupling and parameter efficiency are both priorities. In the presented synthetic benchmarks, deterministic DFT token mixing with lightweight phase shifts provides a useful forecasting signal while substantially reducing trainable parameter count relative to self-attention baselines.

These findings should be interpreted as an efficiency-oriented trade-off rather than a universal accuracy replacement. In our experiments, dense self-attention attains lower test error, while the phasor architecture offers lower parameterization and subquadratic token-mixing complexity. This pattern is consistent with prior efficient-Transformer literature that studies the accuracy-efficiency frontier under constrained budgets [16, 11].

## 7.1 Topological Stability for Infinite Contexts

The phase-constrained state representation provides a useful inductive bias for oscillatory data: states remain bounded and interpretable in angular coordinates. In stacked settings, inter-block pull-back normalization helps maintain controlled phase ranges, which may support stable optimization as depth increases.

At the same time, this manuscript does not establish asymptotic guarantees for arbitrarily long contexts or all training regimes. Empirical validation here is limited to synthetic autoregressive tasks and moderate context lengths. Extending analysis to larger contexts, real-world datasets, and broader optimization settings remains an important next step.

Table 3 defines the theoretical scaling boundaries, comparing parameter counts between Large Phasor Models and explicitly parameterized attention-based Transformers.

Table 3: Parameter scaling comparison: Phasor Transformer vs. standard Transformer for a single block with sequence length  $T$  and embedding dimension  $d$ .

Component	Standard Transformer	Phasor Transformer
Token Mixing	$4d^2$ (QKV + output proj.)	0 (DFT, parameter-free)
Feed-Forward	$8d^2$ (two linear layers)	$2T$ (phase shifts)
<b>Total per block</b>	$\mathcal{O}(d^2)$	$\mathcal{O}(T)$

The reduction from quadratic attention-parameter blocks to linear phase-parameter blocks follows directly from the deterministic DFT mixer. This structural property motivates LPM for settings where deployment constraints and model compactness are central design criteria.

## 8 Conclusion

This work introduced the Large Phasor Model (LPM), a phase-native alternative to attention-heavy sequence modeling that combines trainable shift gates with parameter-free DFT token mixing. Across the reported synthetic forecasting benchmarks, LPM demonstrates a consistent efficiency-oriented profile: substantially lower trainable parameter counts with globally coupled token interaction at  $\mathcal{O}(N \log N)$  mixing complexity.

The empirical results also show the expected trade-off with dense self-attention baselines, which achieve lower error in the tested setup. Therefore, the main contribution of LPM is not replacing attention universally, but establishing a practical design point for compact long-context modeling where geometric phase constraints and deterministic global mixing are desirable.

Future work will evaluate LPM on larger real-world datasets, broader context regimes, and hybrid architectures that combine phasor blocks with selective learned attention to improve the accuracy-efficiency frontier.

## References

- [1] Iz Beltagy, Matthew E. Peters, and Arman Cohan. Longformer: The long-document transformer. *arXiv preprint arXiv:2004.05150*, 2020.
- [2] Tom B. Brown, Benjamin Mann, Nick Ryder, Melanie Subbiah, Jared Kaplan, Prafulla Dhariwal, Arvind Neelakantan, Pranav Shyam, Girish Sastry, Amanda Askell, et al. Language models are few-shot learners. *Advances in Neural Information Processing Systems*, 33:1877–1901, 2020.
- [3] Rewon Child, Scott Gray, Alec Radford, and Ilya Sutskever. Generating long sequences with sparse transformers. *arXiv preprint arXiv:1904.10509*, 2019.

- [4] Krzysztof Choromanski, Valerii Likhoshesterov, David Dohan, Xingyou Song, Andreea Gane, Tamas Sarlos, Peter Hawkins, Jared Davis, Afroz Mohiuddin, Lukasz Kaiser, et al. Rethinking attention with performers. *International Conference on Learning Representations*, 2021.
- [5] Tri Dao, Daniel Y. Fu, Stefano Ermon, Atri Rudra, and Christopher Re. Flashattention: Fast and memory-efficient exact attention with io-awareness. *Advances in Neural Information Processing Systems*, 35:16344–16359, 2022.
- [6] Jacob Devlin, Ming-Wei Chang, Kenton Lee, and Kristina Toutanova. Bert: Pre-training of deep bidirectional transformers for language understanding. *Proceedings of NAACL-HLT*, pages 4171–4186, 2019.
- [7] Alexey Dosovitskiy, Lucas Beyer, Alexander Kolesnikov, Dirk Weissenborn, Xiaohua Zhai, Thomas Unterthiner, Mostafa Dehghani, Matthias Minderer, Georg Heigold, Sylvain Gelly, et al. An image is worth 16x16 words: Transformers for image recognition at scale. *International Conference on Learning Representations*, 2021.
- [8] Akira Hirose. *Complex-Valued Neural Networks: Advances and Applications*. John Wiley & Sons, 2012.
- [9] Jordan Hoffmann, Sebastian Borgeaud, Arthur Mensch, Elena Buchatskaya, Trevor Cai, Eliza Rutherford, Diego de Las Casas, Lisa Anne Hendricks, Johannes Welbl, Aidan Clark, et al. Training compute-optimal large language models. *arXiv preprint arXiv:2203.15556*, 2022.
- [10] Jared Kaplan, Sam McCandlish, Tom Henighan, Tom B. Brown, Benjamin Chess, Rewon Child, Scott Gray, Alec Radford, Jeffrey Wu, and Dario Amodei. Scaling laws for neural language models. *arXiv preprint arXiv:2001.08361*, 2020.
- [11] James Lee-Thorp, Joshua Ainslie, Ilya Eckstein, and Santiago Ontanon. Fnet: Mixing tokens with fourier transforms. *arXiv preprint arXiv:2105.03824*, 2021.
- [12] Bryan Lim, Sercan O. Arik, Nicolas Loeff, and Tomas Pfister. Temporal fusion transformers for interpretable multi-horizon time series forecasting. *International Journal of Forecasting*, 37(4):1748–1764, 2021.
- [13] Yuqi Nie, Nam Nguyen, Phanwadee Sinthong, and Jayant Kalagnanam. A time series is worth 64 words: Long-term forecasting with transformers. *International Conference on Learning Representations*, 2023.
- [14] Tohru Nitta. *Complex-Valued Neural Networks: Utilizing High-Dimensional Parameters*. Information Science Reference, 2009.
- [15] Vasu Sharma. Phasorflow: A python library for unit circle based computing. *arXiv preprint arXiv:2603.15886*, 2026.
- [16] Yi Tay, Mostafa Dehghani, Dara Bahri, and Donald Metzler. Efficient transformers: A survey. *ACM Computing Surveys*, 55(6):1–28, 2022.
- [17] Ashish Vaswani, Noam Shazeer, Niki Parmar, Jakob Uszkoreit, Llion Jones, Aidan N Gomez, Lukasz Kaiser, and Illia Polosukhin. Attention is all you need. *Advances in neural information processing systems*, 30, 2017.
- [18] Sinong Wang, Belinda Z. Li, Madian Khabsa, Han Fang, and Hao Ma. Linformer: Self-attention with linear complexity. *arXiv preprint arXiv:2006.04768*, 2020.

- [19] Haixu Wu, Tao Hu, Yong Liu, Hang Zhou, Jianmin Wang, and Mingsheng Long. Timesnet: Temporal 2d-variation modeling for general time series analysis. *International Conference on Learning Representations*, 2023.
- [20] Haixu Wu, Jiehui Xu, Jianmin Wang, and Mingsheng Long. Autoformer: Decomposition transformers with auto-correlation for long-term series forecasting. *Advances in Neural Information Processing Systems*, 34:22419–22430, 2021.
- [21] Manzil Zaheer, Guru Guruganesh, Avinava Dubey, Joshua Ainslie, Chris Alberti, Santiago Ontanon, Panupong Pham, Anirudh Ravula, Qifan Wang, Li Yang, and Amr Ahmed. Big bird: Transformers for longer sequences. *Advances in Neural Information Processing Systems*, 33:17283–17297, 2020.
- [22] Haoyi Zhou, Shanghang Zhang, Jieqi Peng, Shuai Zhang, Jianxin Li, Hui Xiong, and Wancai Zhang. Informer: Beyond efficient transformer for long sequence time-series forecasting. *Proceedings of AAAI*, 35(12):11106–11115, 2021.
- [23] Tian Zhou, Ziqing Ma, Qingsong Wen, Xue Wang, Liang Sun, and Rong Jin. Fedformer: Frequency enhanced decomposed transformer for long-term series forecasting. *International Conference on Machine Learning*, pages 27268–27286, 2022.